Interactions of Radiation and Convection in Simulated Tropical Cloud Clusters

QIANG FU, STEVEN K. KRUEGER, AND K. N. LIOU

Department of Meteorology/CARSS, University of Utah, Salt Lake City, Utah

(Manuscript received 13 May 1994, in final form 7 September 1994)

ABSTRACT

A two-dimensional cumulus ensemble model is used to study the interactions of radiation and convection in tropical squall cloud clusters. The model includes cloud-scale and mesoscale dynamics, an improved bulk ice microphysics parameterization, and an advanced interactive radiative transfer scheme. The life cycle of a tropical squall line is simulated over a 12-h period using thermodynamic and kinematic initial conditions as well as large-scale advective forcing typical of a GATE Phase III squall cluster environment. The focus is on the interaction and feedback between longwave (or IR) radiation and cloud processes.

It will be shown that clear-sky IR cooling enhances convection and, hence, surface precipitation. Simulation results reveal an increase of surface precipitation by ~15% (~1.7 mm) over a 12-h period due to this clear-sky cooling. With fully interactive IR radiative heating, direct destabilization of clouds via IR radiative top cooling and base warming generates more turbulence and contributes to the longevity and extent of the upper-tropospheric stratiform (anvil) clouds associated with deep convection. The greater extent of anvil clouds decreases the outgoing IR flux at the top of the atmosphere by as much as 20 W m^{-2}.

With fully interactive IR radiative heating, the anvil cirrus reduces the IR cooling of the troposphere with respect to the clear-sky values. This cloud IR radiative forcing has a negative feedback on tropical deep convection, which will be referred to as "anvil cloud IR radiative feedback." This feedback decreases surface precipitation by ~10% (~1.3 mm). It will also be shown that IR radiative processes modify the hydrometeor profiles by affecting convection. On changing the cloud particle size distributions prescribed in radiation calculations, it is further demonstrated that the size distributions significantly influence the convective activity through their effects on the cloud IR radiative forcing.

The impact of clear-air IR cooling and cloud radiative forcing on deep convection is further examined by using the cloud-work function, which is a generalized measure of the moist convective instability in the large-scale environment. The clear-air IR cooling tends to increase the cloud-work function, but the cloud IR radiative forcing tends to reduce it, especially for the deepest clouds.

1. Introduction

Cloud systems influence the large-scale circulation of the atmosphere through radiative effects, thermodynamical consequences of phase changes, turbulent and convective transport, and precipitation. Significant uncertainties exist in the representation of clouds and cloud processes in general circulation models (GCMs). Reliable prediction of global climate change will require a comprehensive understanding of and appropriate parameterizations for different kinds of cloud systems. Among them, tropical deep convection is of primary importance (Riehl and Malkus 1958; Simmons 1982). Moreover, the upper-tropospheric stratiform (anvil) clouds associated with deep convection require more and specific attention because of their importance in climate studies and because of the infancy of the parameterizations for these clouds (Randall 1989; Randall et al. 1989).

Radiative heating plays an important role in the evolution of tropical deep convection. Based on cloud-scale and mesoscale modeling and observational studies, three mechanisms for the interaction of radiation and convection have been proposed: (1) radiative destabilization of the tropical environment (Dudhia 1989); (2) direct destabilization of the upper-tropospheric stratiform clouds via cloud-base warming and cloud-top cooling (Chen and Cotton 1988; Ackerman et al. 1988; Lilly 1988); and (3) production of a secondary circulation by horizontal differential radiative heating between cloudy and clear regions (Gray and Jacobson 1977). The first mechanism is due to the domainwide clear-air radiative cooling above a moist boundary layer, which enhances convection and hence surface precipitation. The second contributes to the longevity of anvil clouds but has little direct effect on precipitation. The third also tends to sustain convection. These mechanisms have been widely used to explain interactions between radiation and convection (Churchill and Houze 1991; Tao et al. 1991, 1993; Miller and Frank 1993; Sui et al. 1994; Chin 1994; Xu and Randall 1995). One aspect of cloud–radiation inter-

Corresponding author address: Dr. Qiang Fu, Dept. of Oceanography, Dalhousie University, Halifax, Nova Scotia B3H 4J1, Canada. E-mail: qfu@atm.dal.ca

action that has not been addressed in these studies, however, is the effect on convection of atmospheric IR warming due to clouds.

Clouds are the most important regulator of both solar and IR radiative fields. By reflecting incoming solar radiation back to space, clouds cool the earth–atmosphere system (solar albedo effect). At the same time, by absorbing IR radiation emitted by the underlying atmosphere and surface and reradiating it to space at colder temperatures, clouds warm the earth–atmosphere system (IR greenhouse effect). Because the atmosphere is relatively transparent to solar radiation, cooling of the system due to the solar albedo effect occurs primarily at the surface. The upper-tropospheric stratiform anvil clouds associated with tropical deep convection produce a strong IR greenhouse effect that is mainly confined within the atmosphere (Ramanathan 1987; Fu and Liou 1993). In the last few years, a term referred to as cloud radiative forcing has been frequently used to denote the effect of clouds on the radiation field. The cloud IR radiative forcing through the atmospheric IR warming effect of anvil clouds could have a significant effect on the evolution of convection.

In this study, we use a two-dimensional cumulus ensemble model (CEM) to examine the interactions between radiation and maritime tropical cloud clusters and to determine the effects of cloud-induced IR heating of the troposphere on convection. A CEM is a cloud-resolving numerical model that covers a large area. It can simulate an ensemble of cumulus clouds and its mesoscale organization. In a CEM, the large-scale advective processes are prescribed. Thus, there is no feedback from the CEM to the large-scale dynamics. However, since the cloud radiative forcing depends on the extent and microphysical properties of anvil clouds produced by convection, there will be feedbacks in the CEM among the anvil cirrus, radiation, and convection. This paper focuses on mesoscale convection–radiation interactions and investigates their impact on the parameters related to large-scale motions. For simplicity, we have restricted our attention to tropical cloud clusters over an ocean with a fixed sea surface temperature. In this circumstance, cloud solar radiative forcing at the surface is absent. We have also confined our study principally to the interaction of IR radiation and cloud processes because the cloud radiative forcing in the atmosphere is dominated by IR radiation (see, e.g., Fu and Liou 1993) and because only IR radiation is present during the nighttime. In addition, the incorporation of the diurnal variation of solar radiation in the model will increase the complexity of the interaction and feedback studies in view of the fact that the large-scale forcing is also a function of time.

To investigate the interactions between radiation and convection in tropical cloud clusters, we perform five simulations that have identical large-scale advective forcing, but we include different interactive radiation fields. Each simulation encompasses the life cycle of a cloud cluster. This series of simulations allows us to examine the effects of clear-sky IR radiative heating, the effects of cloud IR radiative forcing, the sensitivity of cloud-radiation interactions to the cloud particle size distribution, and some of the effects of solar radiative heating. Tropical cloud clusters are usually classified as either squall or nonsquall clusters. We choose to simulate squall cloud clusters because the associated anvil clouds are more extensive in these clusters so that cloud radiative effects become more important. Moreover, due to the effects of vertical wind shear on convection, squall clusters are better organized than nonsquall clusters so that their structure is more reproducible from one simulation to another. This makes comparisons between individual simulations meaningful for squall clusters.

This paper is organized as follows. In section 2, we describe the CEM that includes a bulk microphysics parameterization and an interactive radiation scheme. The design of numerical simulations is described in section 3. The simulation results are presented in section 4. In section 5, we discuss the physical mechanisms associated with cloud–radiation interactions and feedbacks. Finally, summary and conclusions are given in section 6.

2. The model

The CEM that is used for studying the interactions between radiation and convection in tropical cloud clusters should explicitly simulate cloud-scale and mesoscale circulations, parameterize the turbulent fluxes in a general way, and simply specify the large-scale advection (forcing). Ice-phase microphysical processes must be included and the cloud properties that strongly affect the radiative fluxes, such as the extent and ice water content of anvil clouds, should be realistically simulated. The radiative processes also need to be carefully parameterized. Earlier versions of the CEM associated with the present study have been described in detail in Krueger (1988) and Xu and Krueger (1991). The current version includes an improved bulk ice-phase microphysics parameterization and an interactive radiative transfer scheme, which are presented in subsections 2b and 2c following a brief description of the basic features of the CEM.

a. Basic features

The time-dependent and nonhydrostatic CEM is based on the two-dimensional (x–z) anelastic system of equations that includes the Coriolis force. The resulting mesoscale and cloud-scale dynamical equations are coupled with a third-moment turbulence closure. The motivation for using a third-moment turbulence closure is to improve the simulation of turbulent processes in the boundary layer as well as in clouds. Third-

moment closure has a distinct advantage over simpler closures because it is more general. The full set of turbulence equations includes 11 prognostic equations for second moments, 24 prognostic equations for third moments, and one diagnostic equation for the turbulent length scale.

A CEM is designed to resolve many individual cumulus clouds and simulate their mesoscale organization. Since tropical anvils associated with a mesoscale convective system are about 200 km wide, we use a horizontal domain of 512 km with a grid size of 1 km. The depth of the domain is about 18 km and contains 33 levels. In order to provide adequate vertical resolution in the boundary layer, the vertical grid interval ranges from about 100 m near the surface to about 1000 m near 18 km.

The upper and lower boundaries of the CEM are rigid, while the lateral boundaries use the cyclic boundary condition. The lower boundary in this study is the sea surface, which is characterized by its specified temperature and roughness. The surface turbulent fluxes are calculated from flux-profile relationships following Deardorff's (1972) approach.

In the Tropics, large-scale vertical advection is the primary modulator of cumulus convection on synoptic timescales (Yanai et al. 1976; Lord 1982). For this reason, the CEM includes prescribed large-scale advective tendencies of potential temperature and water vapor.

b. *Microphysics parameterization*

The present model utilizes a bulk method to represent the cloud microphysical processes in which the hydrometeors are categorized into five types: cloud droplets, ice crystals, raindrops, snow, and graupel. Although the parameterized cloud microphysics largely follows Lin et al. (1983) and Lord et al. (1984), we have recently improved the ice phase parameterizations so that the microphysical processes that occur in tropical cloud clusters can be more realistically simulated (Fu et al. 1994; Krueger et al. 1995). Major modifications have been made to the growth of cloud ice by the Bergeron process, the conversion of cloud ice to snow, and the characteristics of graupel. The amount of cloud ice and the extent of anvil cirrus are increased to more realistic values by these changes.

Ice water contents (IWCs) in the upper-tropospheric stratiform clouds are one of the most important cloud properties that determine the atmospheric radiation budget and the heating rate profile within anvils (Ackerman et al. 1988; Fu and Liou 1993). We have used a one-dimensional version of CEM to evaluate the improved microphysics parameterization. We turn off cloud dynamics and turbulence, which leads to a kinematic model in which the air motion pattern is fixed in the simulation. The model inputs are profiles of vertical velocity, temperature, pressure, and water vapor mixing ratio. The initial thermodynamic state is based on the GATE Phase III mean sounding. The prescribed vertical velocity profile is typical of the air motion pattern in the stratiform region associated with a tropical squall line (Rutledge 1986; Gamache and Houze 1982). The simulation time is 24 hours, and the time step is 10 seconds. The model produces a distribution of IWCs and temperatures that are in equilibrium with the air motion pattern.

Variations in the simulated and observed IWCs as functions of temperature and vertical velocity are shown in Fig. 1. The curves are taken from the parameterization results presented by Heymsfield and Donner (1990) for applications to GCMs. IWCs determined from measurements and model simulations are partitioned into vertical velocity intervals. The small symbols are based on measurements obtained in the Tropics presented by these authors. The large symbols are the simulation results based on Lord's original microphysics scheme (Fig. 1a) and the improved microphysics parameterization (Fig. 1b). IWCs computed from Lord's scheme are about one order smaller than the measured values (Fig. 1a). IWCs computed from the present parameterization are much improved and comparable with the measured data, as shown in Fig. 1b.

c. *Radiative transfer parameterization*

The radiative transfer parameterization scheme for application to a mesoscale cloud model is based on the delta-four-stream approximation (Liou et al. 1988) in both solar and thermal infrared wavelengths. For IR wavelengths, the Planck function is expressed in terms of the optical depth in an exponential form. By dividing the atmosphere into a number of homogeneous layers with respect to the single scattering albedo and phase function and by using the boundary conditions and the internal continuity requirements (Liou 1975), the delta-four-stream scheme can be used to calculate the flux distribution. In the resulting matrix formulation, one-third of the elements in the diagonal band of the coefficient matrix are zero. We have developed a numerically stable technique to solve the system of linear equations, which is significantly faster than the standard routines available in the IMSL or LAPACK libraries. The delta-four-stream scheme has an accuracy within ~5% for all atmospheric conditions with reference to results computed from the "exact" adding method for radiative transfer.

Six solar and 12 IR bands are used in the radiation code to resolve the variations in the refractive indices of ice and water and to account for the gaseous absorption. The nongray gaseous absorption due to H_2O, CO_2, O_3, CH_4, and N_2O is incorporated in the scattering model by using the correlated k-distribution approach (Fu and Liou 1992). The continuum absorption of H_2O and the overlap between H_2O and CO_2 are carefully treated in the infrared. Using the correlated k-dis-

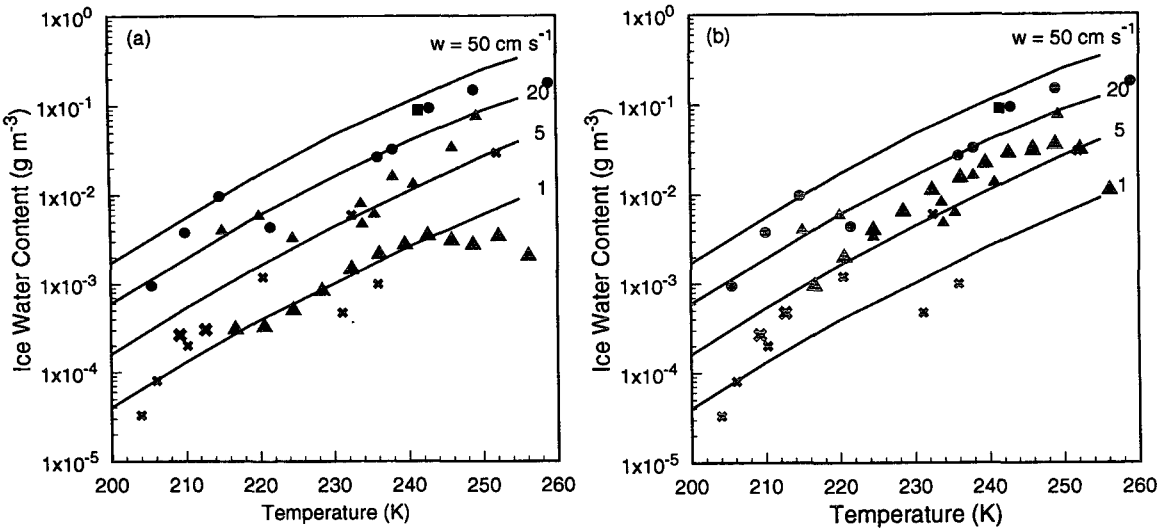

FIG. 1. Ice water content as a function of the temperature and vertical air velocity. The curves are from the parameterization presented by Heymsfield and Donner (1990) for GCMs. The smaller symbols correspond to measured data in tropical conditions taken from the same paper. The bigger symbols are from model simulations by using (a) Lord's original microphysics scheme and (b) the improved microphysics scheme. Crosses: 0–2.5 cm s^{-1}; triangles: 2.5–10 cm s^{-1}; circles: 10–33 cm s^{-1}; squares: >33 cm s^{-1}.

tribution method, 121 spectral calculations are required for each vertical profile. The accuracy of the parameterization for nongray gaseous absorption has been checked with the results computed from a line-by-line program. For all gases, the differences in heating rates are less than 0.05 K day^{-1}, while those in fluxes are less than 1 W m^{-2}.

In conjunction with the radiative transfer scheme, the single-scattering properties, including the extinction coefficient, single scattering albedo, and phase-function expansion coefficients, for each hydrometeor species are efficiently parameterized. For hexagonal ice crystals, the parameterization is made in terms of the mean effective size and IWC based on "exact" results using 11 observed ice crystal size distributions (Fu and Liou 1993). In the "exact" calculations, the geometric ray-tracing program for hexagonal ice crystals (Takano and Liou 1989) is used for size parameters greater than 30, while the exact scattering program for spheroids is employed for size parameters less than 30. For water clouds, a parameterization for the single-scattering properties is developed based on Mie calculations using the observed water droplet size distributions (Fu 1991) in terms of cloud liquid water content and mean effective radius. For rain, snow, and graupel, which are assumed to be spherical particles, truncated constant-slope gamma distributions (Manton and Cotton 1977) are used in Mie calculations. The single-scattering properties of rain, snow, and graupel depend only on their water contents.

To reduce the computational time, the radiation code has been vectorized by placing the loop over the atmospheric columns as the most inner loop. In this manner, radiation calculations can be performed for many model columns simultaneously. For example, on a CRAY Y-MP8/864, the vectorized radiation code is called once for every 64 columns for maximum vectorization efficiency. After vectorizing the code, the computer time for radiation calculations using a CRAY Y-MP8/864 has been reduced by a factor of about 10.

The model top for the radiation calculations is set at 60 km, and two additional levels at 21 and 60 km are added above the CEM model top of 18 km. Temperature, water vapor, and ozone profiles at 21 km are assumed to be the same as those of the standard tropical atmosphere. The mixing ratios of H_2O and O_3 at 60 km are determined by equating the pathlengths between 21 and 60 km and those obtained from the detailed tropical atmospheric profile. The temperature at 60 km is set at 240 K, which is the average temperature between 21 and 60 km. The differences in heating rates below 18 km between the values obtained from the detailed profile above the cloud model domain and those computed from only two levels are within 0.02 K day^{-1}.

The average IR heating rate for the lowest model layer is extremely sensitive to the surface air temperature and water vapor mixing ratio. Based on numerical experiments, these values must be obtained from the surface layer similarity profiles at a height z (in meters), which can be expressed as

$$z = 0.2766 + 0.2324 \ln|L|, \qquad (2.1)$$

where L is the Monin–Obukhov length (in meters).

The potential temperature and water vapor at any height z within the surface layer can be obtained from their values at the surface and at $z = z_m$, the first CEM

level height above the surface. Using the flux profile relationships (Deardorff 1972), we have

$$\theta(z) = \theta_s - (\theta_s - \theta_m)C(z_m)/C(z) \quad (2.2)$$

and

$$q_v(z) = q_{vs} - (q_{vs} - q_{vm})C(z_m)/C(z), \quad (2.3)$$

where θ_s is the potential temperature corresponding to the sea surface temperature, q_{vs} is the saturation mixing ratio at this temperature, and θ_m and q_{vm} are the CEM potential temperature and mixing ratio values at $z = z_m$. The similarity function for the unstable surface layer is

$$C^{-1}(z) = \frac{0.74}{\kappa}\left[\ln\left(\frac{z}{z_0}\right) - 2\ln\left(\frac{1+y}{2}\right)\right], \quad (2.4)$$

where $y = (1 - 9\zeta)^{1/2}$, $\zeta = z/L$, κ is the von Karman constant (0.35), and z_0 is the roughness length. Based on GATE data, typical values for z_0 and L are 2×10^{-4} m and -5 m, respectively.

3. Design of the numerical experiment

We have designed a series of five numerical simulations to examine the interactions of longwave radiation and cloud processes. In simulation R1, radiative heating is not included in the thermodynamic equation. We may, however, compute the radiation field diagnostically from the model fields. Simulation R2 includes only the clear-sky IR radiative heating. By comparing results from R2 and R1, radiative destabilization of the tropical environment due to the domainwide clear-air radiative cooling can be studied. In simulation R3, fully interactive IR radiative heating is included. Since the bulk microphysics parameterization does not provide information on cloud particle size distributions, we must prescribe the mean effective size for ice particles (D_e) and the mean effective radius of cloud droplets (r_e), which are required in the radiation code. In simulation R3, we set $D_e = 25$ μm and $r_e = 5$ μm: values within the range of the observed data (Fu and Liou 1993; Knollenberg et al. 1993; Fu 1991). Comparing results from R3 and R2, the effect of cloud radiative forcing on convection and on the longevity and extent of anvil clouds via cloud base warming and top cooling can be investigated. Here R4 is identical to R3 except that the prescribed mean effective particle sizes are larger. As shown by Fu and Liou (1993), the cloud radiative forcing is very sensitive to the cloud particle size distribution. In simulation R4, we set $D_e = 125$ μm and $r_e = 12$ μm: values also within the range of the observed data. This experiment is designed to study the sensitivity of cloud particle size distribution to cloud-radiation interactions that has not been explored previously. The final simulation R5 includes fully interactive net (IR + solar) radiative heating. The prescribed D_e and r_e in the radiation calculations are the same as those in R4. For solar radiation, the cosine of the solar zenith angle is set as 0.5 and the solar constant is 1365 W m^{-2}, representing the average day–time condition. The five numerical experiments are summarized and listed in Table 1.

The initial thermodynamic state for all simulations is based on the GATE Phase III mean sounding (Fig. 2a). The geostropic (and initial) horizontal wind profile normal to the squall line (Fig. 2b) is obtained from a 6-h average from 4.75 to 5 days of the Q04 simulation presented by Xu et al. (1992). This profile resembles the 11 September 1974 squall line environment observed during GATE Phase III (Sui and Yanai 1986). The wind profile favors the formation of a long-lasting squall line system. The large-scale advective cooling and moistening profiles (Fig. 2c) are the same as those used in the Q04 simulation. The large-scale advective forcing is typical of the GATE Phase III disturbed periods. The initial thermodynamic state, the initial wind field, and the imposed large-scale advective forcing are horizontally uniform. The simulation time is 12 hours, with a time step of 10 seconds. The large-scale forcing is applied constantly for the first four hours and decreases to zero during the next four hours according to a cosine function that has a period of eight hours. For the last four hours, the large-scale forcing remains zero. The sea surface temperature is fixed at 299.9 K, and the Coriolis parameter for 15°N is used.

The convection is initiated by a low-level cool pool (Tao et al. 1991) that is gradually introduced over 10 minutes after the first 60 minutes of integration. Following Tao et al., the cool pool is 45 km wide and 3 km deep (from the surface to the dry layer near 700 mb), which is vertically but not horizontally uniform. The dependence on horizontal location x can be expressed as follows:

$$\left(\frac{\partial\theta}{\partial t}\right)_{cp} = \begin{cases} \left(\dfrac{\partial\theta}{\partial t}\right)_{cpmax} \ln\eta(x)/\ln 0.25, \\ \qquad\qquad \text{for} \quad x_1 \leq x \leq x_2 \\ 0 \quad \text{otherwise,} \end{cases} \quad (3.1)$$

where

$$\eta(x) = \frac{0.75}{x_2 - x_1}(x - x_1) + 0.25. \quad (3.2)$$

TABLE 1. Summary of the numerical simulations.

R1:	Without radiation
R2:	With clear-sky IR radiation
R3:	With fully interactive IR radiation: $D_e = 25$ μm, $r_e = 5$ μm
R4:	With fully interactive IR radiation: $D_e = 125$ μm, $r_e = 12$ μm
R5:	With fully interactive net (IR + solar) radiation: $D_e = 125$ μm, $r_e = 12$ μm; $\mu_0 = 0.5$, $S = 1365$ W m^{-2}

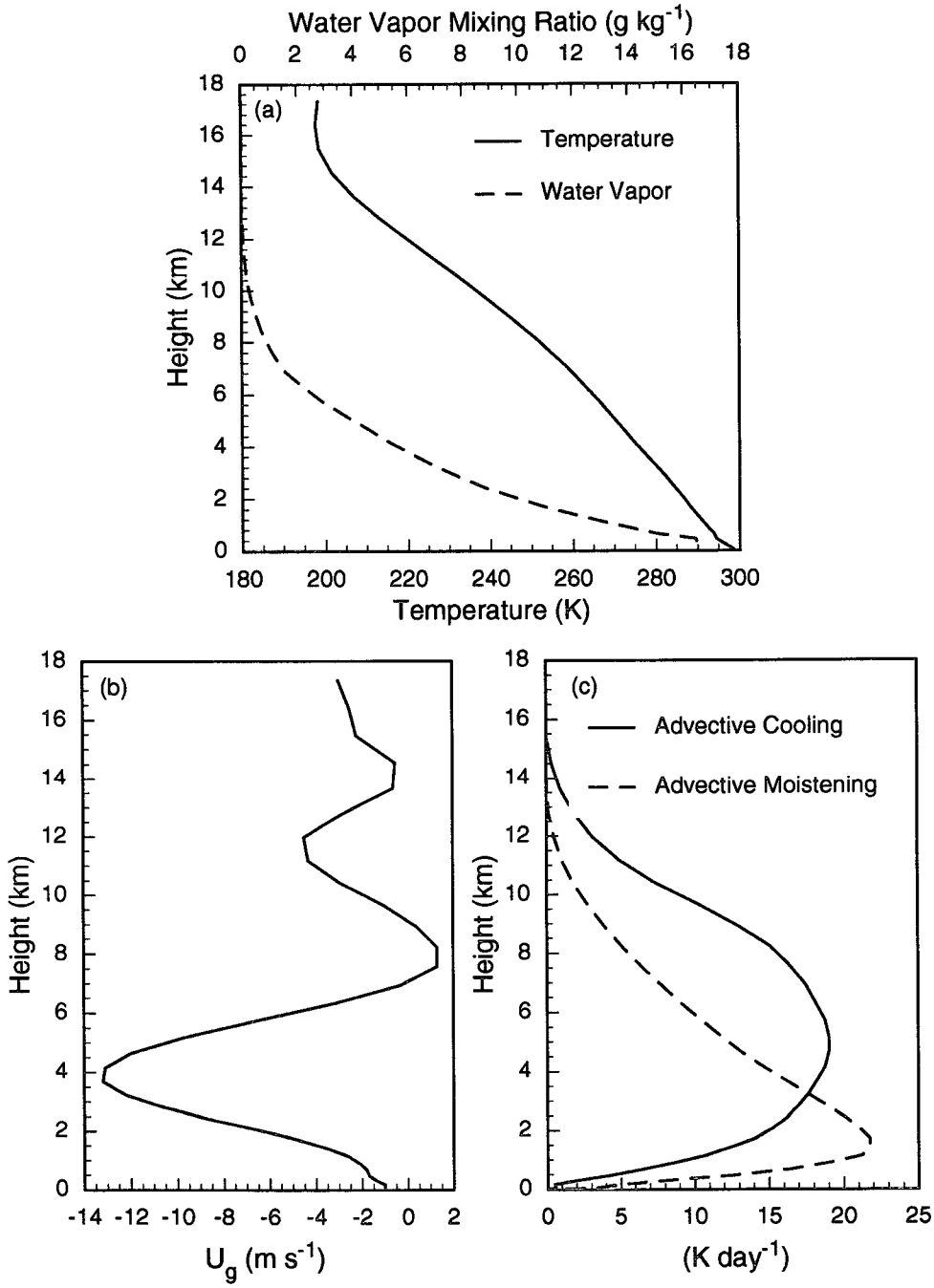

FIG. 2. (a) Initial thermodynamic sounding, (b) initial horizontal wind profile normal to the squall line, and (c) imposed large-scale advective cooling (solid line) and moistening effects (dashed line) for the first 240-min simulation time.

In these equations θ is the potential temperature; x_1 is the location where $(\partial\theta/\partial t)_{cp} = (\partial\theta/\partial t)_{cpmax}$; x_2 is the location where $(\partial\theta/\partial t)_{cp} = 0$; and $(\partial\theta/\partial t)_{cpmax} = 0.00875$ K s^{-1}. The maximum cooling rate is at $x = x_1$ since the squall line system propagates toward smaller x with the wind profile imposed.

The radiative fields are calculated every minute, that is, every six dynamical time steps during which interval the radiative heating rates remain constant. Because the propagation speed of the squall line is ~12 m s^{-1} (Fu et al. 1994), the system moves about 720 m per minute, which is less than the horizontal grid size of 1000 m.

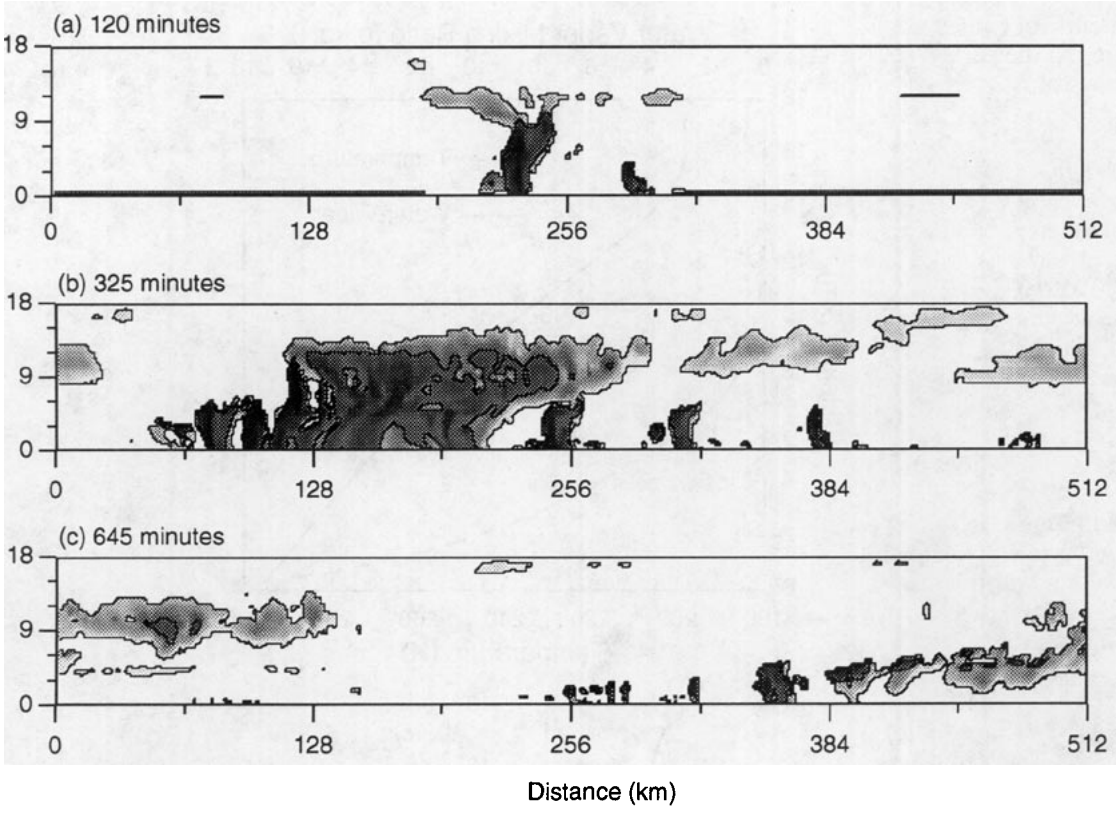

FIG. 3. Snapshots ($x-z$ sections) of the total hydrometeor mixing ratio, including cloud water, cloud ice, rain, snow, and graupel at (a) 120, (b) 325, and (c) 645 minutes. The gray scale is linear to the logarithm of mixing ratio: black and white represent mixing ratios larger than 10^{-2} and smaller than 10^{-6}, respectively. Contours for values of 10^{-6} and 10^{-4} are shown in the figure.

Thus, during one minute, the cloud system will largely remain in the same grid boxes. The radiation calculations use the thermodynamic and bulk hydrometeor fields provided from the CEM. The ozone profile is taken from the standard tropical atmosphere. For CO_2, CH_4, and N_2O, uniform mixing ratios are assumed throughout the atmosphere with concentrations of 330, 1.6, and 0.28 ppmv, respectively.

In strong convective regions, atmospheric temperatures and humidities are directly affected by the presence of convection. In simulation R2, the clear-sky radiative heating rates are computed from thermodynamic profiles in the squall line environment at $x = 324$ km. The evolution of these profiles is largely determined by the large-scale advective forcing and the subsiding motion in the environment due to convection. These processes tend to balance, so the thermodynamic profiles in the environment differ only slightly from the initial ones.

As mentioned in the Introduction, Gray and Jacobson (1977) proposed the secondary circulation generated by horizontal differential radiative heating between cloudy and clear regions that can assist in sustaining convection. However, the studies by Miller and Frank (1993) and Xu and Randall (1995) suggested that this cloud-induced secondary circulation plays a relatively minor role in modulating tropical convection. A recent study by Wong and Stephens (1994) concluded that the strength of this circulation is a function of both the vertical wind shear profile and the low-level stability of the environment. They found that the cloud-induced secondary circulation is strongest when the vertical wind shear is weak. As the wind shear increases, the secondary circulation weakens. Thus, it is expected that the Gray–Jacobson mechanism is insignificant in our simulations because of the presence of strong vertical wind shear.

4. Results from the numerical simulations

The structure of the simulated squall cloud cluster's hydrometeor fields is first examined. Figure 3 shows snapshots of the total hydrometeor mixing ratio, including cloud water, ice, rain, snow, and graupel, based on the R3 simulation at three different times. The logarithm of the mixing ratio is denoted by a linear gray scale: black represents mixing ratios larger than 10^{-2}, and white represents mixing ratios smaller than 10^{-6}.

Contours for values of 10^{-6} and 10^{-4} are shown in the figure. At the earlier time (Fig. 3a), the cloud cluster consists of isolated precipitating convective towers. In the mature stage (Fig. 3b), the anvil cloud associated with the mesoscale convective system has a horizontal scale of ~180 km, which extends from the front to the back of the system. The system moves westward (from right to left) at an average speed of 12 m s^{-1} and consists of significant precipitation that covers a region of ~140 km. The deep cumulonimbi continually propagate into the ambient air ahead where new growth occurs, while older towers successively join the main anvil mass (Zipser 1977). In the dissipating stage (Fig. 3c), little precipitation remains, and the upper-tropospheric stratiform clouds are thinning and breaking up (Houze 1982). The typical life cycle and structure of a cloud cluster (e.g., Leary and Houze 1979) can be seen in Fig. 3. In the following, we discuss the cloud-radiation interactions based on numerical simulations beginning with the cloud-top temperature, which can be directly related to infrared satellite imagery.

a. *Cloud-top temperature*

Figures 4a (from R1 with no radiative heating), 4b (from R2 with only clear-sky IR radiative heating), and 4c (from R3 with fully interactive IR radiative heating) show the time evolution of the cloud-top temperature, indicated by a linear gray scale: white for 200 K and black for 300 K. The cloud-top temperature is defined here as the temperature at the first level to which the "suspended water" path from the model top exceeds 0.1 kg m^{-2}. "Suspended water" includes cloud water, cloud ice, and snow. Cirrus anvils associated with the squall line appear light gray. Several significant features are shown in Fig. 4. First, the cloud-top temperature in Fig. 4b is generally lower than that in Fig. 4a, which indicates that clear-sky IR radiation enhances convection. Second, the anvil clouds with interactive IR radiation (Fig. 4c) appear to last longer. Third, by comparing Fig. 4c to Fig. 4b, convective activity appears to dissipate faster due to cloud radiative forcing. To examine these features, we show the time–height cross sections of the domain averages of the radiative heating rates in Fig. 5. The contour interval is 0.5 K day^{-1}, with positive values shaded. Figures 5a and 5b contain the radiative heating rates for R2 and R3, respectively. In Fig. 5c, the cloud radiative forcing is obtained by taking the differences between Fig. 5b and Fig. 5a.

Basically, the differences between R2 and R1 simulations are caused by clear-sky radiative heating rates (Fig. 5a), while those between R3 and R2 are due to the cloud radiative forcing (Fig. 5c). Consistent with the results presented by Dudhia (1989), clear-air radiative cooling (Fig. 5a) enhances convection, as shown in Fig. 4. The cloud radiative forcing pattern between ~10.5 and ~13.5 km displayed in Fig. 5c is due to radiative cloud-base warming and cloud-top cooling, which contributes to the longevity of anvil clouds through direct radiative destabilization. Before ~4 hours, strong cooling at cloud tops (Fig. 5c) can also enhance shallow convection. After that time, the cloud radiative forcing tends to warm the whole troposphere due to the presence of extensive sheets of anvil clouds. We hypothesize that the atmospheric IR warming effect of clouds has a negative feedback on deep convection. The physical basis of this hypothesis will be examined in section 5.

b. *Surface precipitation*

The surface precipitation can be used as a proxy for deep convection (Gray and Jacobson 1977; Xu et al. 1992). Figure 6 presents the time series of domain total surface precipitation. The results from R1 are denoted by the solid line, R2 by the dashed line, and R3 by the dotted line. The difference between R2 and R1 is due to clear-sky IR radiation. It is evident that the domain-wide clear-air radiative cooling in the troposphere increases surface precipitation. This increase is ~15% (i.e., ~1.7 mm) over the 12-h simulation. The difference between R3 and R2 is due to the cloud IR radiative forcing, which decreases surface precipitation. This is especially evident after ~6.5 hours. The response of surface precipitation to cloud radiative warming appears to exhibit a time lag. In the present simulations, there is ~10% (i.e., ~1.3 mm) decrease of surface precipitation due to cloud IR radiative forcing. The domain total precipitation from R3 is slightly larger than R2's before ~4.5 hours (Fig. 6) due to the direct radiative destabilization of cloud layers. Based on these results we conclude that the clear-air IR radiative cooling enhances convection, while the cloud IR radiative forcing suppresses convection.

c. *Convective heating and convective drying*

The goal of cumulus parameterization is to determine the convective heating ($Q_1 - Q_R$) and convective drying Q_2 profiles, where Q_R is the radiative heating rate, and Q_1 and Q_2 are the apparent heat source and the apparent moisture sink of a large-scale system (Yanai et al. 1973). Here ($Q_1 - Q_R$) and Q_2 are directly related to the contributions of convective effects, which can be explicitly calculated by the CEM.

The convective heating and drying profiles in R1 represent the response of the cumulus ensemble to the advective forcing alone, which is prescribed and assumed to be the same for all simulations. The convective heating and drying profiles in R2 and R3 represent the response not only to the advective forcing but also to the radiative processes. Figures 7a–d present the time- and domain-averaged profiles of ($Q_1 - Q_R$), Q_R, Q_1, and Q_2, respectively. By comparing these profiles for R2 and R1 shown in Figs. 7a and 7d, we find that

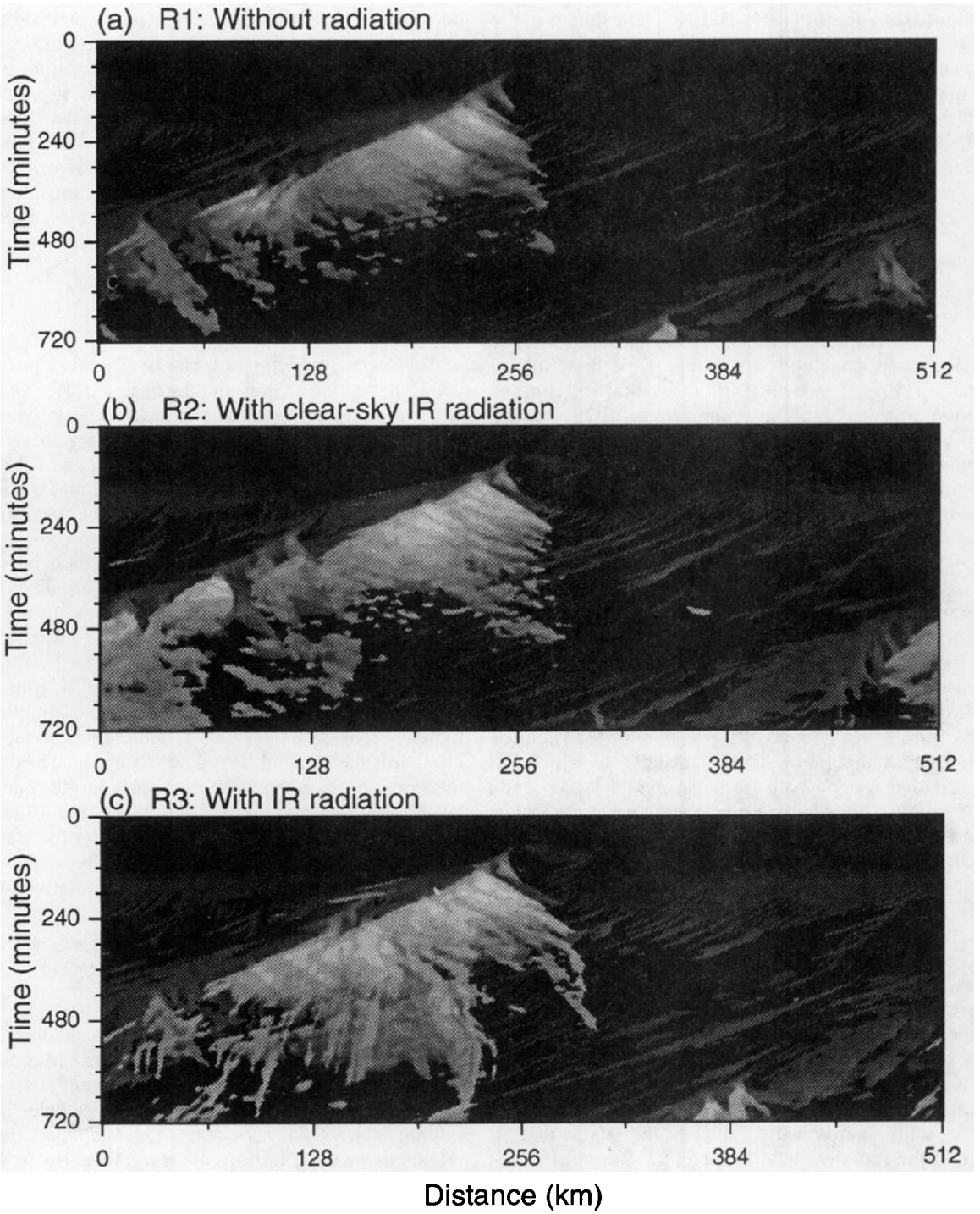

FIG. 4. Hovmöller diagrams (x–t sections) of the cloud-top temperature for (a) R1, (b) R2, and (c) R3. The cloud-top temperature is shown by a linear gray scale: white represents 200 K; black represents 300 K.

($Q_1 - Q_R$) and Q_2 significantly increase in response to clear-sky IR radiative cooling (see Q_R for R2 in Fig. 7b). However, the cloud radiative forcing, that is, the difference between Q_R for R3 and R2 (Fig. 7b), tends to warm and has the opposite effect throughout the low and middle troposphere. By comparing the results from R3 and R2, as shown in Figs. 7a and 7d, it is seen that the cloud IR radiative forcing tends to suppress con-

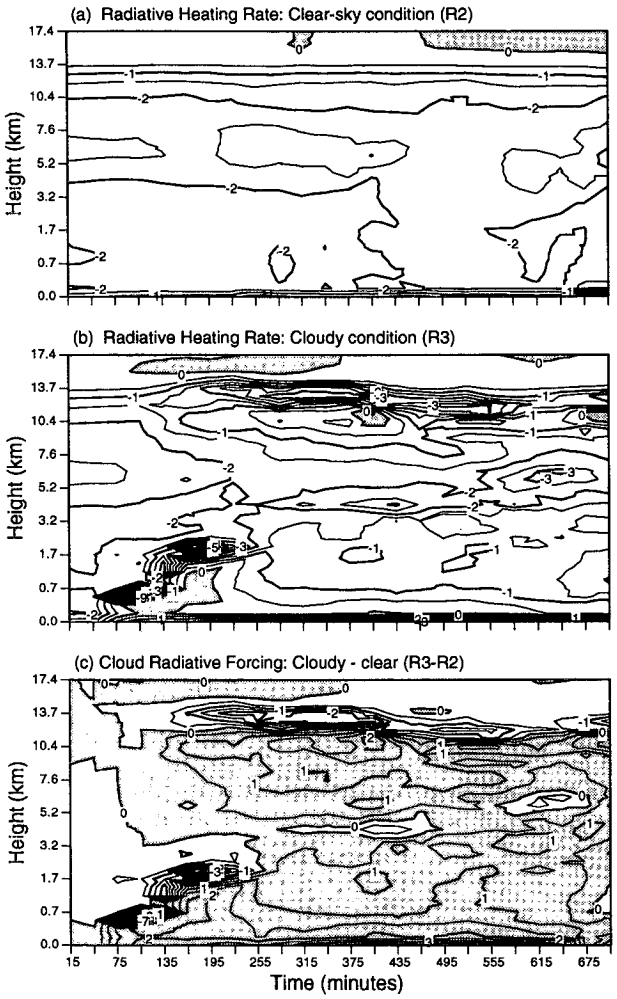

FIG. 5. Time–height cross section for the domain-averaged radiative heating rates. The contour interval is 0.5 K day^{-1}, with positive values shaded. Panels (a) and (b) are for radiative heating rates in the cases of R2 and R3, respectively. In (c), the cloud radiative forcing is calculated by taking the difference between the two cases.

vective activity. In the upper troposphere, however, this forcing produces a slight increase in convective activity because convective overturning develops within the large stratiform anvil clouds. This is associated with the direct radiative destabilization. In Fig. 7b we find that cloud radiative forcing tends to cool the cloud top relative to cloud base.

Figure 8 shows the time- and domain-averaged profiles of (a) temperature and (b) water vapor mixing ratio deviations with respect to initial conditions. The thermodynamic changes result from the combined effects of large-scale cooling, radiative heating, and convective heating. The apparent heating (Fig. 7c) is the combined result of radiative and convective heating. Both clear-sky IR radiation and cloud radiative forcing play an important role in the thermodynamic changes because the large-scale cooling and apparent heating, despite their relatively large magnitudes, tend to balance. The water vapor mixing ratio changes are caused by large-scale moistening and apparent drying (convective drying). Radiation affects the water vapor profile through convection. It is significant above ~2 km. Below ~7 km, the clear-sky IR cooling tends to dry the atmosphere. The opposite is true for cloud radiative forcing. Above ~7 km, the cloud radiative forcing drys the atmosphere because of direct radiative destabilization. From the results presented in Fig. 8, the impact of radiation (including both direct and indirect effects) on temperature and water vapor mixing ratio deviations are significant compared with the deviations in the case without radiation. It is clear that the radiative heating rate and its effects on convective heating and drying must be reliably accounted for in the parameterization of apparent heating and drying profiles that are crucial in climate modeling studies.

d. Cloud characteristics and outgoing IR flux

One of the most important quantities for climate studies is the outgoing IR flux at the top of the atmosphere. This flux is strongly modulated by the cloud amount, cloud-top height, and hydrometeor water content. We shall first investigate the impact of cloud-radiation interactions on cloud fields.

Figure 9a illustrates time- and domain-averaged cloud amount profiles. The definition of cloud amount in a CEM grid box (1 km wide) follows Xu and Krueger (1991). The maximum cloud amounts occur at ~12 km for all three cases. They are 0.40, 0.43, and

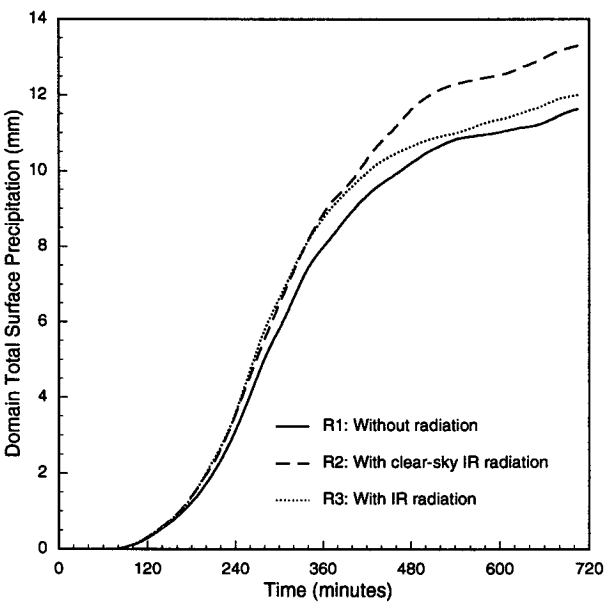

FIG. 6. Domain total amount of surface precipitation as a function of time. The solid, dashed, and dotted lines are from runs R1, R2, and R3, respectively.

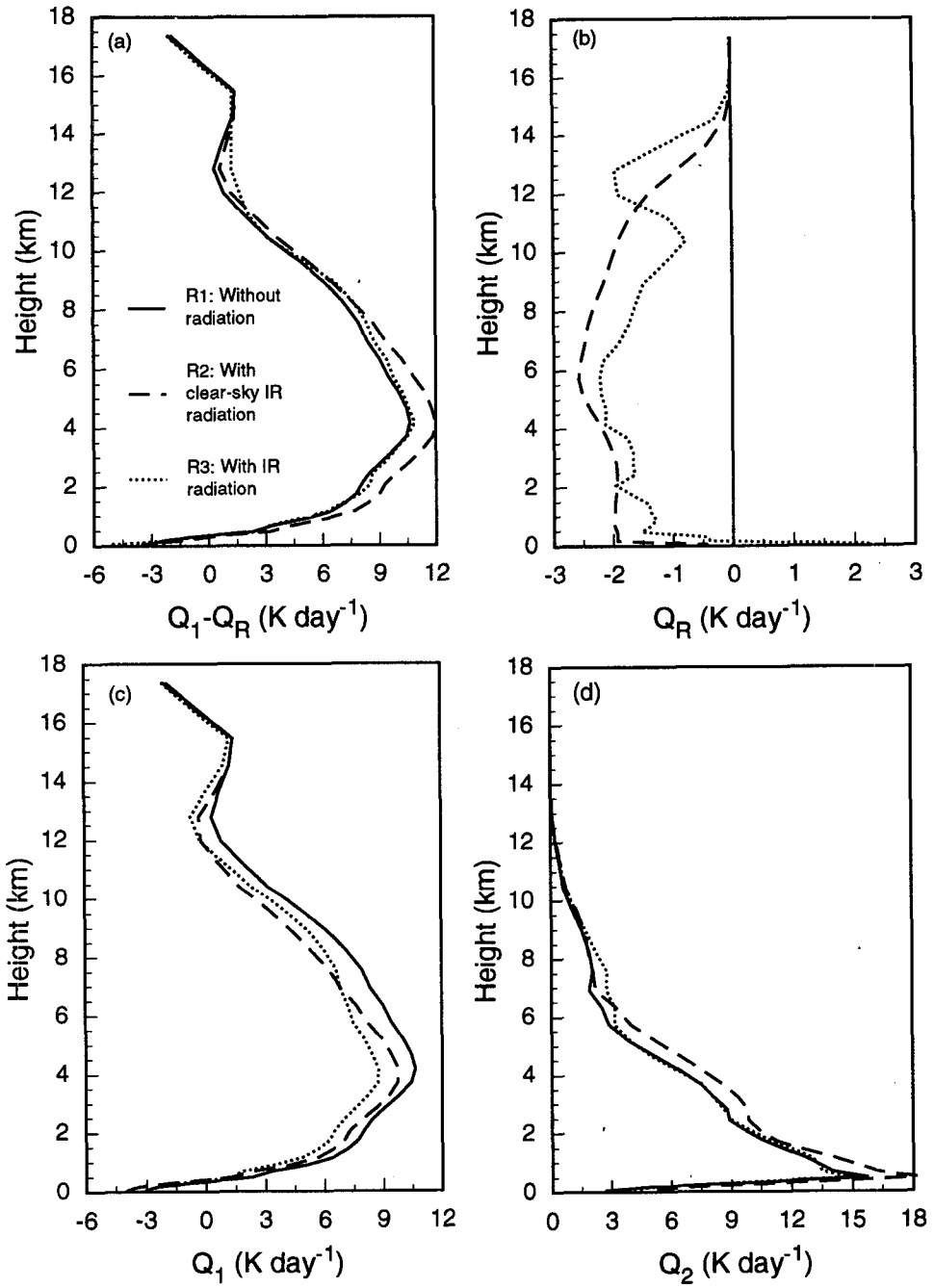

FIG. 7. Time- and domain-averaged profiles of (a) convective heating ($Q_1 - Q_R$), (b) radiative heating Q_R, (c) apparent heating Q_1, and (d) apparent (or convective) drying Q_2. The solid, dashed, and dotted lines are from runs R1, R2, and R3, respectively.

0.52 for R1, R2, and R3, respectively. The clear-sky IR cooling tends to increase the cloud amount throughout the atmosphere. The most interesting feature of Fig. 9a is that the cloud IR radiative forcing increases the anvil cloud amount significantly (~21%). This is due to the direct radiative destabilization via cloud-base warming and cloud-top cooling, which increases cloud longevity. Lilly (1988) proposed that the in-cloud radiative destabilization generates buoyant turbulence in anvil clouds and contributes to their longevity. Figure 9b shows the time- and domain-averaged profiles of turbulent kinetic energy (TKE). Compared with results

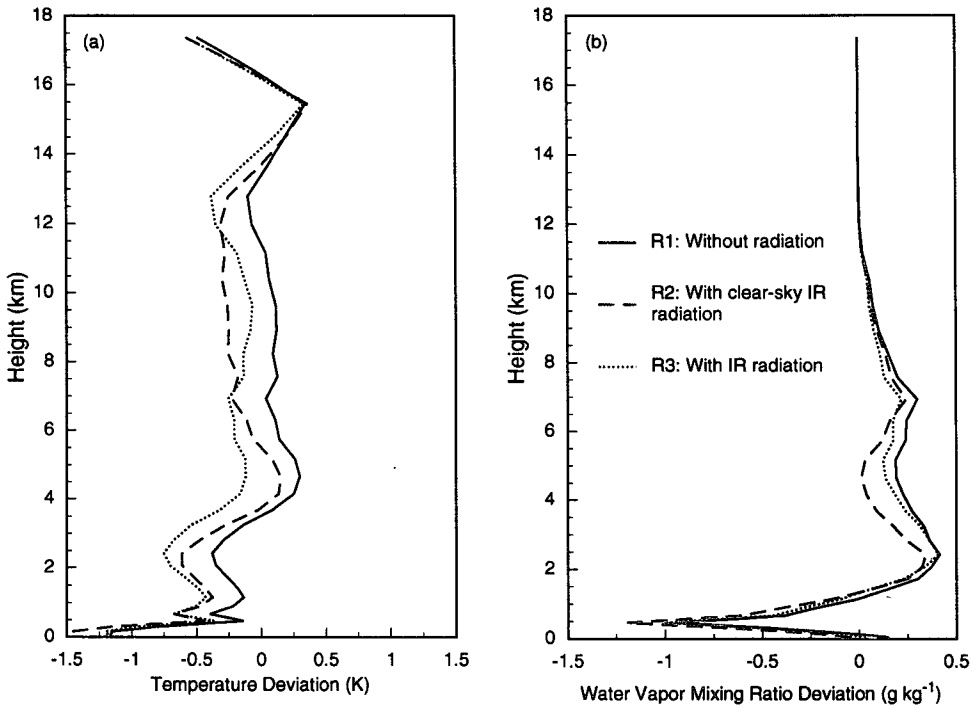

FIG. 8. Time and domain average of (a) the temperature deviation and (b) the water vapor mixing ratio deviation, with respect to initial conditions.

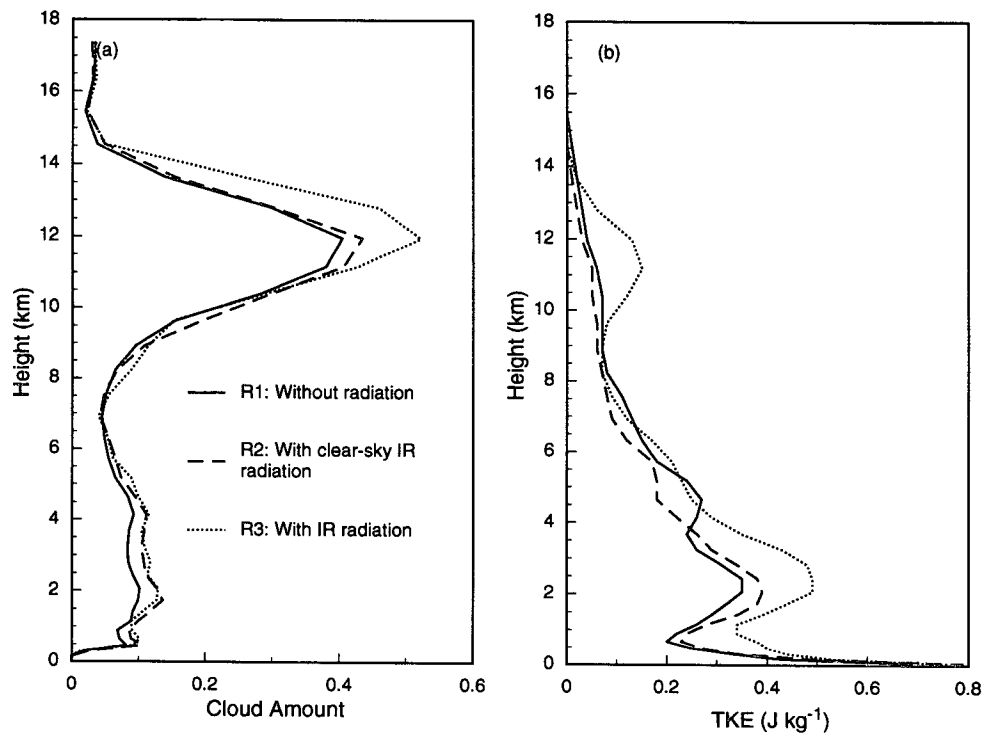

FIG. 9. Time and domain average of (a) cloud amount and (b) turbulent kinetic energy profiles.

from R1 and R2, the dotted line from R3 (with fully interactive IR radiation) is generally larger, especially at ~11.5 km. The preceding results are consistent with Lilly's theory. The significant increase of TKE at ~2 km for R3 is also due to the direct radiative destabilization. It is clear from Fig. 9a that cloud-radiation interactions significantly modulate the cloud fields, especially the upper-tropospheric stratiform clouds.

The effects of radiation on the hydrometeor fields are also significant. Figures 10a and 10b show the time and domain average of mixing ratio profiles for cloud water plus cloud ice and snow plus graupel plus rain, respectively. Clear-air IR cooling is associated with the changes in the cloud and precipitating hydrometeor profiles. It is interesting to note that the cloud radiative forcing reduces the mixing ratio of precipitating particles throughout the atmosphere. However, it has more limited impact on the cloud water and ice mixing ratio profiles. By comparing the results presented in Fig. 10a and Fig. 9a, it is evident that the anvil cloud amount is not necessarily related to cloud ice water mixing ratio (or content).

To examine the impact of convective–radiative interactions on the outgoing IR flux at the top of the atmosphere, we calculate this flux using the radiation code and the cloud thermodynamic and bulk hydrometeor fields generated from R1, R2, and R3. This flux is referred to here as the diagnostic flux. The time- and domain-averaged outgoing IR fluxes are 225.8, 221.9, and 216.9 W m^{-2} for R1, R2, and R3, respectively. The clear-sky IR cooling decreases the outgoing IR flux by ~3.9 W m^{-2}, while the cloud radiative forcing further decreases this flux by ~5.0 W m^{-2}. Convection–radiation interactions modulate the outgoing IR flux at the top of the atmosphere mainly through their effect on the extent of anvil clouds (Fig. 9a). The time series of domain-averaged outgoing fluxes at the top of the atmosphere are shown in Fig. 11. The difference between R1 and R3 is as large as 20 W m^{-2}; a result of the longevity of anvil clouds associated with the direct radiative destabilization.

e. Effects of cloud particle size distribution and solar radiation

In light of the preceding discussion, it is clear that the cloud IR radiative forcing stabilizes convection significantly. It has been noted that the cloud IR radiative forcing is very sensitive to the cloud particle size distribution (e.g., Fig. 9a of Fu and Liou 1993). Consequently, the evolution of tropical mesoscale systems and tropical rainfall will depend on the cloud particle size distribution through convection–radiation interactions. Note that in the cloud microphysics parameterization, only ice/liquid water contents are involved. Runs R3 and R4 both include fully interactive IR radiation but use different mean effective sizes and effective radii for ice and water cloud particles in the

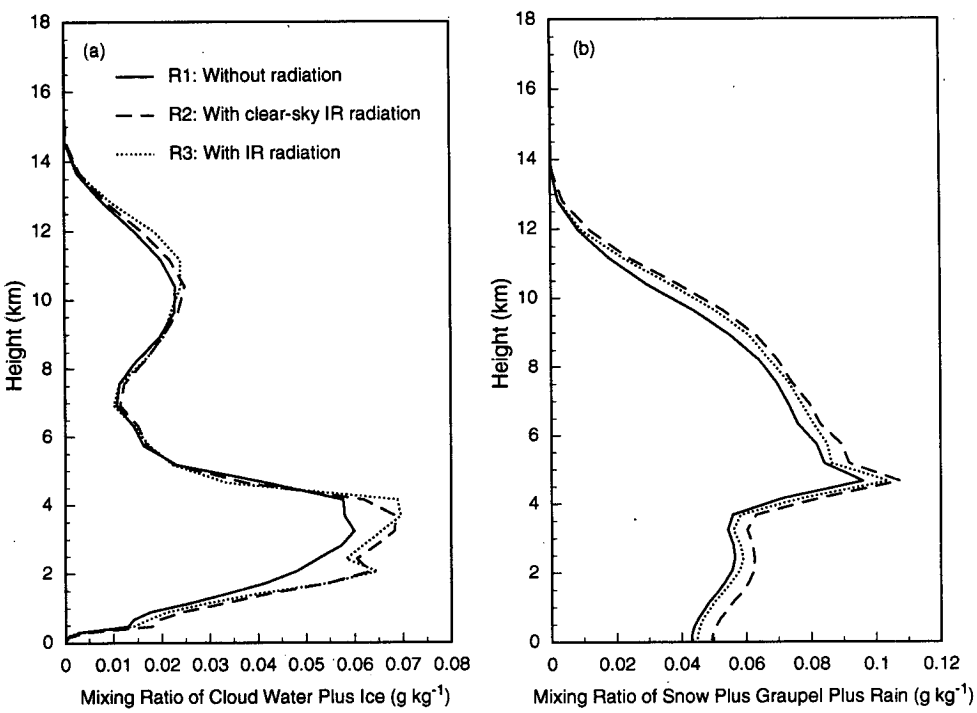

FIG. 10. Time- and domain-averaged mixing ratio profiles for (a) cloud water plus cloud ice and (b) snow plus graupel plus rain.

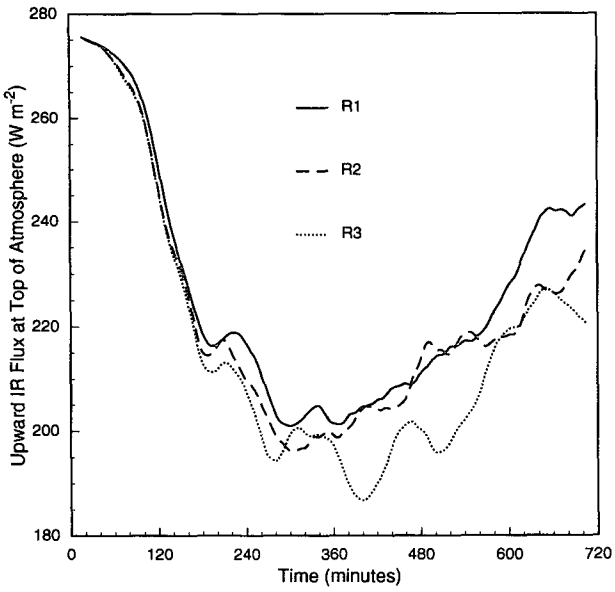

FIG. 11. Time series of the domain-averaged outgoing IR flux at the top of the atmosphere. The fluxes are computed from the radiation code using the thermodynamic and bulk hydrometeor fields simulated from R1 (solid line), R2 (dashed line), and R3 (dotted line).

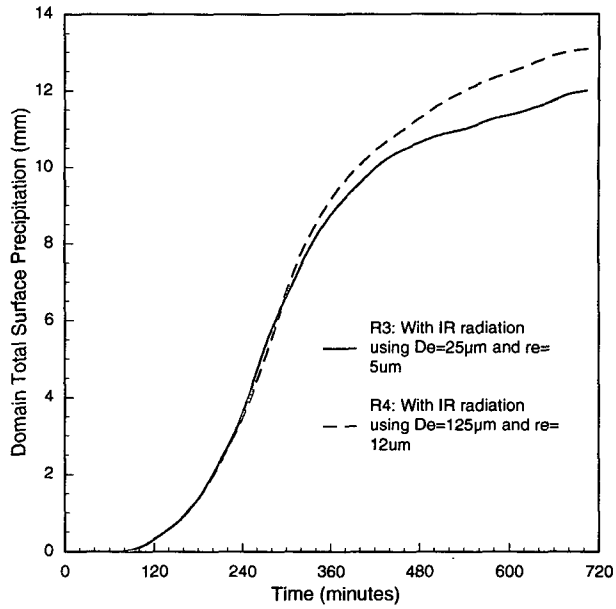

FIG. 12. Domain total amount of the surface precipitation as a function of time for the 12-h simulations. Results using different mean effective sizes in the simulations are denoted by the solid line (R3) and the dashed line (R4), respectively.

radiation calculations. Figure 12 shows the domain total surface precipitation as a function of time for R3 (solid line) and R4 (dashed line). Because clouds containing larger mean effective sizes absorb less longwave radiation, the atmospheric radiative warming effect of such clouds is reduced, leading to stronger convection and more surface precipitation. On the other hand, the direct destabilization of cloud layers is weaker in R4, leading to a slight decrease in surface precipitation before 4.5 hours. The present study suggests that cloud particle size distributions in the radiation calculation should be realistically specified or predicted by cloud models to investigate cloud–radiation interactions.

The effect of solar heating in the atmosphere on surface precipitation is shown in Fig. 13. In this case, atmospheric solar heating decreases surface precipitation because the domainwide clear-air solar warming in the troposphere reduces the total radiative cooling rate and consequently tends to suppress convection. The solar heating also reduces the cloud direct destabilization effects produced by IR radiation flux exchanges because the solar heating rate peaks at the cloud top (Ackerman et al. 1988).

In this section, we have examined the impact of cloud–radiation interactions on the macroscopic behavior of a cloud cluster. It should be noted that five simulations presented herein are for the same cloud system under different radiative forcings. In order to minimize high-frequency variability effects due to the somewhat random growth of individual convective cells between the simulations, we have chosen to simulate a well-organized squall cloud cluster associated with the strong vertical wind shear so that its general structure and evolution are reproducible from one sim-

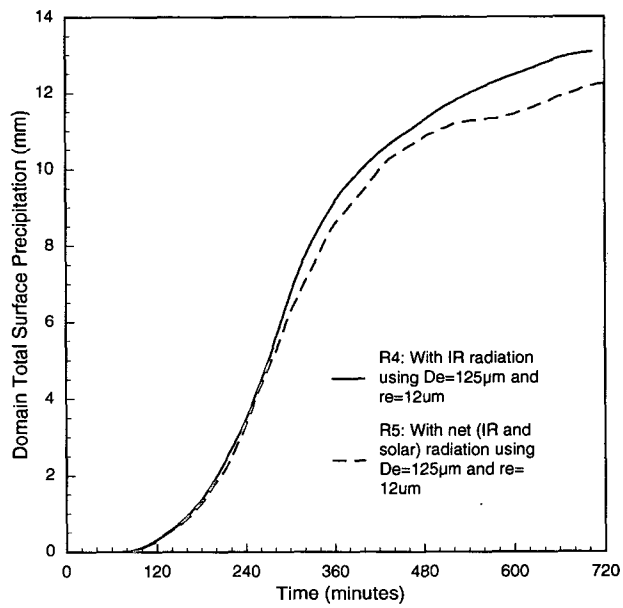

FIG. 13. Domain total amount of the surface precipitation as a function of time. Results with IR and net (IR + solar) radiation in the simulations are denoted by the solid line (R4) and the dashed line (R5), respectively.

ulation to another. In our simulations, the large-scale forcing is also strong, which has the controlling and modulating effects upon the growth of individual cells (Xu et al. 1992). To initiate the cloud cluster, we have used a cool pool instead of random perturbation (Krueger 1988; Xu and Krueger 1991). The significance of cloud–radiation interactions can be recognized in terms of the macroscopic behavior of the cloud cluster (e.g., surface precipitation, apparent heating and drying profiles, cloud cover, etc.), which are critical to climate studies.

5. Mechanisms for convection–radiation interactions

In the present study, the life cycle of a tropical squall cloud cluster has been simulated. We have investigated interactions between radiation and convection in the simulated cloud cluster. The results suggest that radiation has a significant impact on the macroscopic behavior of cumulus ensembles.

As summarized in the Introduction, previous explanations for mesoscale cloud–radiation interactions can be grouped into three basic categories: destabilization of the environment due to clear-air radiative cooling, direct destabilization of anvil clouds via cloud-base warming and cloud-top cooling, and production of a secondary circulation by horizontal differential radiative heating between cloudy and clear regions. All of these mechanisms tend to enhance convection. The first two are significant in our simulations, but the third is less important as discussed in section 3. The mechanism associated with the suppression of convection due to the atmospheric IR warming effect of clouds, however, has not been previously investigated. Our results reveal that this mechanism plays a significant role during the mature stage of the cloud cluster during which an upper-tropospheric stratiform anvil shield develops and covers an extensive area.

Direct destabilization of anvil clouds via cloud-base warming and cloud-top cooling is confirmed to be important for upper-tropospheric stratiform clouds. This mechanism mainly contributes to the longevity of these clouds in line with the findings presented by Dudhia (1989), Churchill and Houze (1991), and Xu and Randall (1995). Our results also reveal that direct destabilization prolongs the lifetime of anvil clouds by generating more turbulence in these clouds, in agreement with the theory proposed by Danielson (1982) and Lilly (1988).

The primary effect of clear-air IR cooling is to destabilize the troposphere and enhance deep convection. However, cloud IR radiative forcing tends to stabilize the atmosphere. Destabilization is related to an increase of the vertically integrated buoyancy of a parcel that rises from the subcloud layer (the layer below cumulus cloud base) to its nonbuoyancy level. Destabilization can occur by warming or moistening the subcloud layer where the parcel originates and by cooling or moistening the atmosphere above cloud base. Over a region with a fixed SST, such as considered in this study, destabilization is due primarily to cooling or moistening of the atmosphere above cloud base. Over such a region, any process that tends to cool the atmosphere is "destabilizing," while the reverse is true for any process that tends to warm the atmosphere. In the following, we examine the destabilizing effects of clear-air radiative cooling and the stabilizing effects of cloud IR radiative forcing on deep convection by using the cloud-work function.

The cloud-work function is a generalized measure of the moist convective instability in the large-scale environment. It is defined as the cumulus cloud subensemble kinetic energy generation (per unit cloud-base mass flux) due to work done by the buoyancy force (Arakawa and Schubert 1974; Lord and Arakawa 1980; Lord 1982; Lord et al. 1982). It is given by

$$A(z_t) = \int_{z_b}^{z_t} \frac{g}{\bar{\theta}(z)} e^{\lambda(z_t)(z-z_b)} \{\theta_{vc}[z, \lambda(z_t)] - \bar{\theta}_v(z)\} dz, \tag{5.1}$$

where z_t is the cloud-top height (defined as the nonbuoyancy level), z_b is the cloud-base height, g is the gravitational acceleration, $\bar{\theta}$ is the environmental potential temperature, θ_{vc} and $\bar{\theta}_v$ are the subensemble and environmental virtual potential temperatures, respectively, and λ is the fractional entrainment rate determined by the cloud-top nonbuoyancy condition. In Eq. (5.1), $g(\theta_{vc} - \bar{\theta}_v)/\bar{\theta}$ is the buoyancy force. Therefore, A is an integral measure of the buoyancy force with the weighting function $e^{\lambda(z-z_b)}$, representing the normalized cloud-mass flux. The cloud-work function is a property of the thermodynamic structure of the large-scale environment. An increase in $A(z_t)$ corresponds to destabilization for clouds with cloud tops at $z = z_t$, while a decrease corresponds to stabilization. The cloud-work function may increase or decrease due to large-scale advection, radiation, and surface fluxes. Cumulus convection usually tends to decrease the cloud-work function.

To calculate the destabilization due to large-scale advection and radiation, we calculate dA/dt due to those processes alone. In the computation of the cloud-work function, we use the domain-average temperature and water vapor mixing ratio profiles stored at 5-min interval from runs R1, R2, and R3. These data are then averaged over 30 minutes to produce "observation" of the environmental profiles. From each of these profiles, the cloud-work function $A(z_t)$ is calculated for clouds with different cloud-top heights z_t. The cloud base is fixed at 500 m. The temperature and water vapor mixing ratio profiles modified by the prescribed large-scale advective cooling and moistening and the radiative heating from R1, R2, and R3 simulations in a time interval Δt are then used to compute a new cloud-work

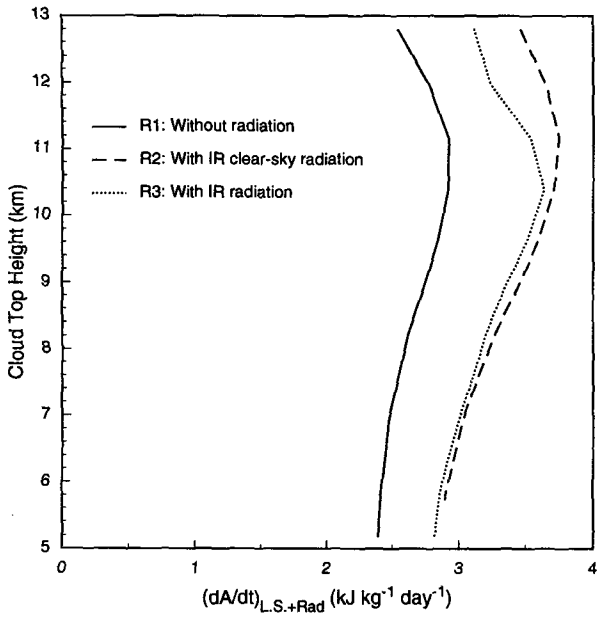

FIG. 14. Time and domain average of the time derivative of the cloud-work function due to the large-scale advection and radiation. The ordinate is the cloud-top height in kilometers. The solid, dashed, and dotted lines are for R1, R2, and R3, respectively.

function $A'(z_t)$. It follows that the time derivative of the cloud-work function can be written as

$$\left(\frac{dA}{dt}\right)_{\text{L.S.+Rad}} = \frac{A'(z_t) - A(z_t)}{\Delta t}, \qquad (5.2)$$

where Δt is set as 30 minutes.

Figure 14 shows the 12-h-averaged dA/dt for R1, R2, and R3 as a function of cloud-top height. The solid line is for results due solely to the prescribed advective cooling and moistening (R1). Because the cloud-work function tends to increase, the large-scale advection tends to destabilize the cloud system and to increase the moist convective instability. Clear-air radiative cooling (R2) significantly increases dA/dt, the rate of increase of moist convective instability, as shown by the dashed line. However, the cloud radiative forcing, that is, the atmospheric radiative warming effect of clouds, decreases dA/dt, especially for deep convection. Because there is typically a near-balance (i.e., quasi equilibrium) between the generation of moist convective instability and its destruction by cumulus clouds (Arakawa and Schubert 1974), we conclude that the differences in destabilization rate produced by radiative forcing result in the differences in the intensity of convection.

Lord (1982) used the Arakawa-Schubert cumulus parameterization (i.e., quasi equilibrium) to investigate the sensitivity of the time-averaged precipitation rate to the prescribed radiative heating rate profiles during GATE Phase III. Using cooling rate profiles for a clear atmosphere and for an atmosphere with 100% cirrus cover, Lord found that the time-averaged precipitation rate for the cloudy case was 23% less than the rate for the clear case over an 18-day period. The difference is mainly due to cloud IR forcing because the impact of cloud solar forcing is primarily at the surface. The radiative heating rate profile produced from simulation R3 lies between those of the clear and cloud (100%) profiles. In R3, the surface precipitation decreases by ~10% due to cloud radiative forcing consistent with Lord's results.

Figure 15 is a schematic illustration of the interactions between radiation and convection in tropical

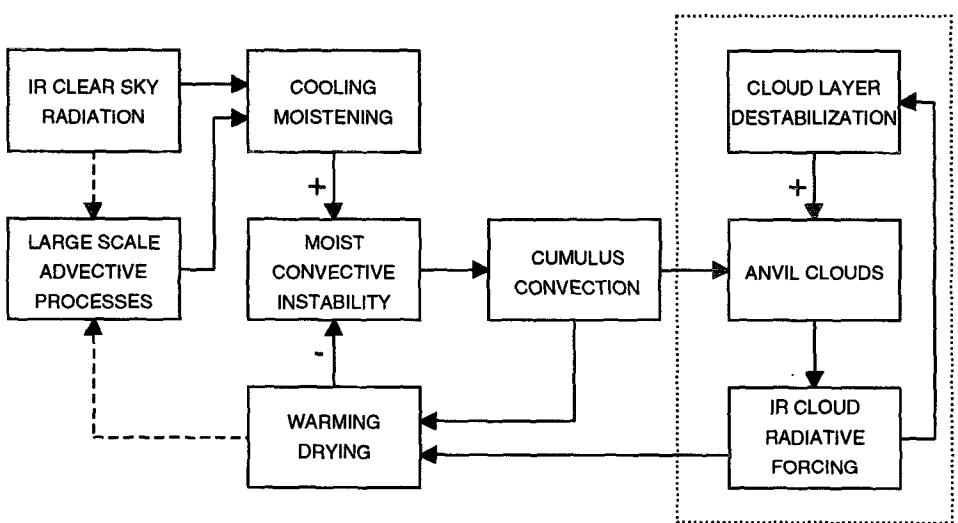

FIG. 15. A schematic illustration of mesoscale radiative–convective interactions and feedbacks. The dashed lines are feedbacks that have not been included in the present CEM.

squall cloud clusters based on simulation results. Cumulus convection is forced by the large-scale advective cooling and moistening. The clear-air IR radiation cools the atmosphere and augments the convective response to the advective forcing. A cumulus ensemble affects its large-scale environment primarily by compensating subsidence (Arakawa and Schubert 1974). The subsidence warms and dries the environment, leading to a negative feedback on convection. The anvil clouds produced by convection reduce the IR radiative cooling, warm the troposphere, and produce a negative feedback on moist convective instability, which is referred to as "anvil cloud IR radiative feedback." At the same time, the IR cloud radiative forcing has a positive feedback on the anvil clouds via cloud-top cooling and cloud-base warming. This feedback destabilizes the anvil clouds, promotes convective overturning within the cloud layer, and increases the longevity of anvil clouds. As a result, the atmospheric IR warming effect of anvil clouds increases, leading to a greater negative feedback to moist convective instability.

The present study represents the first attempt to examine the IR warming effect of clouds on deep convection using a cumulus ensemble model. We have demonstrated that the stabilization of deep convection is significantly influenced by the cloud-warming effect. Since the microphysics, thermodynamics, and dynamics in cloud systems may vary substantially between different types of mesoscale convective systems (MCSs), the importance of the preceding mechanisms for cloud–radiation interactions may also vary for different types of tropical MCSs. For example, the IR radiative feedback associated with anvil clouds is a result of their atmospheric IR warming effect. This warming effect is related to the cloud macrophysical (anvil cloud cover and cloud height) and microphysical (IWC and D_e) properties. These properties vary substantially for convective systems with different structures of organization (e.g., in nonsquall or squall cloud clusters), which may lead to varying quantitative aspects of the anvil cloud IR radiative feedback. With known anvil microphysical properties and cloud height, variation in the anvil cloud IR radiative feedback is proportional to the cloud cover. Finally, it should be noted that feedbacks of cumulus convection and radiative processes to large-scale motions, denoted by dashed lines in Fig. 15, are not included in the present CEM. In a GCM, the mesoscale convective–radiative feedbacks are confined to a single column. Thus, in order to include these feedbacks in a GCM, it is important to develop appropriate and consistent parameterizations for cumulus convection, anvil clouds, and radiative transfer processes.

6. Summary and conclusions

A two-dimensional CEM has been used to investigate the effects of cloud–radiation interactions on a simulated tropical MCS. The model includes a modified ice-phase bulk microphysics parameterization and an advanced radiation code. The microphysics parameterization has been used to determine the microphysical tendencies of hydrometeors (cloud ice, cloud water, rain, snow, and graupel). The simulated IWCs in tropical conditions compare reasonably well with aircraft observed values. We have also incorporated in the CEM a state of the art radiation program that integrates in a coherent manner the delta-four-stream approximation for radiative transfer, the correlated k-distribution method for nongray gaseous absorption, and the parameterizations of the single-scattering properties for hydrometeors. The radiation code is fully interactive with microphysics, turbulence, and cloud dynamics.

The life cycle of a tropical squall line has been simulated over a 12-h period by using thermodynamic and kinematic initial conditions and large-scale forcing typical of a GATE Phase III squall cluster environment. A number of numerical simulations have been designed to examine the mechanisms for cloud-radiation interactions, including runs without incorporating radiative heating, with clear-air IR radiative heating, and with fully interactive IR and net radiative transfer programs. The main results are summarized as follows.

(1) Clear-air radiative cooling enhances convection and, hence, surface precipitation. In the present study, the surface precipitation over a 12-h period increases by ~15% (1.7 mm). The cooling also leads to increases in convective heating ($Q_1 - Q_R$) and convective drying Q_2 and changes the hydrometeor profiles.

(2) Direct destabilization of clouds via cloud-top cooling and cloud-base warming contributes to the longevity of anvil cirrus and to the increase in cloud cover. Because of this increase, the outgoing IR flux at the top of the atmosphere can be reduced by as much as 20 W m^{-2}. Radiative destabilization prolongs cirrus clouds by generating more turbulence.

(3) Cloud IR radiative forcing associated with anvils in the atmosphere acts to suppress the tropical deep convection and decreases surface precipitation. The present study shows a 10% (1.3 mm) decrease associated with this process, which we refer to as "anvil cloud IR radiative feedback."

(4) The particle size distributions in clouds play a significant role in cloud–radiation interactions. Clouds containing larger mean effective sizes/radii would have smaller cloud IR radiative forcing and less effect on suppressing convection. This suggests that cloud particle size distributions should be simulated simultaneously in order to understand more comprehensively interactions among radiative heating, cloud microphysics, and dynamics processes in a cloud model.

The effects of clear-air IR cooling and cloud IR radiative forcing on deep convection are further examined by using the cloud-work function, which is a generalized measure of the moist convective instability in

the large-scale environment. Clear-air IR cooling increases the cloud-work function, but the cloud IR radiative forcing tends to reduce it, especially for the deepest clouds. The present study represents the first attempt to examine the impact of cloud IR radiative forcing on deep convection by using a CEM. In particular, we have provided a fundamental understanding of the role of upper-tropospheric stratiform clouds associated with deep convection in the interactions between radiation and convection. Such an understanding is essential for the parameterization of these clouds in climate models.

Acknowledgments. The research work contained herein was supported by AFOSR Grant 91-0039 and in part by NASA Grant NAG5-1050 and NSF Grant ATM 90-24217. Numerical computations for this work were performed on the CRAY Y-MP8/864 computer at the National Center for Atmospheric Research. We thank Dr. S. Chin of the Lawrence Livermore Laboratory for useful discussions and Dr. N. Rao for assistance in preparing the diagrams presented in the text.

REFERENCES

Ackerman, T. P., K. N. Liou, F. P. J. Valero, and L. Pfister, 1988: Heating rates in tropical anvils. *J. Atmos. Sci.*, **45**, 1606–1623.

Arakawa, A., and W. H. Schubert, 1974: Interaction of a cumulus cloud ensemble with the large-scale environment. Part I. *J. Atmos. Sci.*, **31**, 674–701.

Chen, S., and W. R. Cotton, 1988: The sensitivity of a simulated extratropical mesoscale convective system to longwave radiation and ice-phase microphysics. *J. Atmos. Sci.*, **45**, 3897–3910.

Chin, H. N. S., 1994: The impact of the ice phase and radiation on a midlatitude squall line. *J. Atmos. Sci.*, **51**, 3320–3343.

Churchill, D. D., and R. A. Houze Jr., 1991: Effects of radiation and turbulence on the diabatic heating and water budget of the stratiform region of a tropical cloud cluster. *J. Atmos. Sci.*, **48**, 903–922.

Danielson, E. F., 1982: A dehydration mechanism for the stratosphere. *Geophys. Res. Lett.*, **9**, 605–608.

Deardorff, J. W., 1972: Parameterization of the planetary boundary layer for use in general circulation models. *Mon. Wea. Rev.*, **100**, 93–106.

Dudhia, J., 1989: Numerical study of convection observed during the winter monsoon experiment using a mesoscale two-dimensional model. *J. Atmos. Sci.*, **46**, 3077–3107.

Fu, Q., 1991: Parameterization of radiative processes in vertically non-homogeneous multiple scattering atmospheres. Ph.D. Dissertation, University of Utah, 259 pp.

——, and K. N. Liou, 1992: On the correlated *k*-distribution method for radiative transfer in nonhomogeneous atmospheres. *J. Atmos. Sci.*, **49**, 2139–2156.

——, and ——, 1993: Parameterization of the radiative properties of cirrus clouds. *J. Atmos. Sci.*, **50**, 2008–2025.

——, ——, and S. K. Krueger, 1994: Cloud–radiation interactions in tropical anvils. *Proc., Sixth Conf. on Climate Variations*, Nashville, TN, Amer. Meteor. Soc., 235–239.

Gamache, J. F., and R. A. Houze Jr., 1982: Mesoscale air motions associated with a tropical squall line. *Mon. Wea. Rev.*, **110**, 118–135.

Gray, W. M., and R. W. Jacobson Jr., 1977: Diurnal variation of deep cumulus convection. *Mon. Wea. Rev.*, **105**, 1171–1188.

Heymsfield, A. J., and L. J. Donner, 1990: A scheme for parameterizing ice-cloud water content in general circulation models. *J. Atmos. Sci.*, **47**, 1865–1877.

Houze, R. A., Jr., 1982: Cloud clusters and large-scale vertical motions in the tropics. *J. Meteor. Soc. Japan*, **60**, 396–410.

Knollenberg, R. G., K. Kelly, and J. C. Wilson, 1993: Measurements of high number densities of ice crystals in the tops of tropical cumulonimbus. *J. Geophys. Res.*, **98**, 8639–8664.

Krueger, S. K., 1988: Numerical simulation of tropical cumulus clouds and their interaction with the subcloud layer. *J. Atmos. Sci.*, **45**, 2221–2250.

——, Q. Fu, K. N. Liou, and H.-N. S. Chin, 1995: Improvement of an ice-phase microphysics parameterization for use in numerical simulations of tropical convection. *J. Appl. Meteor.*, **34**, 281–287.

Leary, C. A., and R. A. Houze Jr., 1979: The structure and evolution of convection in a tropical cloud cluster. *J. Atmos. Sci.*, **36**, 437–457.

Lilly, D. K., 1988: Cirrus outflow dynamics. *J. Atmos. Sci.*, **45**, 1594–1605.

Lin, Y. L., R. D. Farley, and H. D. Orville, 1983: Bulk parameterization of the snow field in a cloud model. *J. Climate Appl. Meteor.*, **22**, 1065–1092.

Liou, K. N., 1975: Applications of the discrete-ordinate method for radiative transfer to inhomogeneous aerosol atmospheres. *J. Geophys. Res.*, **80**, 3434–3440.

——, Q. Fu, and T. P. Ackerman, 1988: A simple formulation of the delta-four-stream approximation for radiative transfer parameterizations. *J. Atmos. Sci.*, **45**, 1940–1947.

Lord, S. J., 1982: Interaction of a cumulus cloud ensemble with the large-scale environment. Part III: Semiprognostic test of the Arakawa-Schubert cumulus parameterization. *J. Atmos. Sci.*, **39**, 88–103.

——, and A. Arakawa, 1980: Interaction of a cumulus cloud ensemble with the large-scale environment. Part II. *J. Atmos. Sci.*, **37**, 2677–2692.

——, W. C. Chao, and A. Arakawa, 1982: Interaction of a cumulus cloud ensemble with the large-scale environment. Part IV: The discrete model. *J. Atmos. Sci.*, **39**, 104–113.

——, H. E. Willoughby, and J. M. Piotrowicz, 1984: Role of a parameterized ice-phase microphysics in an axisymmetric, nonhydrostatic tropical cyclone model. *J. Atmos. Sci.*, **41**, 2836–2848.

Manton, M. J., and W. R. Cotton, 1977: Formulation of approximate equations for modeling moist deep convection on the mesoscale. Atmospheric Science Paper No. 266, Dept. of Atmospheric Science, Colorado State University, Fort Collins, CO, 62 pp.

Miller, R. A., and W. M. Frank, 1993: Radiative Forcing of simulated tropical cloud clusters. *Mon. Wea. Rev.*, **121**, 482–498.

Ramanathan, V., 1987: The role of earth radiation budget studies in climate and general circulation research. *J. Geophys. Res.*, **92**, 4075–4095.

Randall, D. A., 1989: Cloud parameterization for climate modeling: Status and prospects. *Atmos. Res.*, **23**, 345–361.

——, Harshvardahan, D. A. Dazlich, and T. G. Corsetti, 1989: Interactions among radiation, convection, and large-scale dynamics in a general circulation model. *J. Atmos. Sci.*, **46**, 1943–1970.

Riehl, H., and J. S. Malkus, 1958: On the heat balance in the equatorial trough zone. *Geophysica*, **6**, 503–538.

Rutledge, S. A., 1986: A diagnostic modeling study of the stratiform region associated with a tropical squall line. *J. Atmos. Sci.*, **43**, 1356–1377.

Simmons, A. J., 1982: The forcing of stationary wave motion by tropical diabatic heating. *Quart. J. Roy. Meteor. Soc.*, **108**, 503–534.

Sui, C. H., and M. Yanai, 1986: Cumulus ensemble effects on the large-scale vorticity and momentum fields of GATE. Part I: Observational evidence. *J. Atmos. Sci.*, **43**, 1618–1642.

——, K. M. Lau, W. K. Tao, and J. Simpson, 1994: The tropical water and energy cycles in a cumulus ensemble model. Part I: Equilibrium climate. *J. Atmos. Sci.*, **51,** 711–728.

Takano, Y., and K. N. Liou, 1989: Radiative transfer in cirrus clouds. Part I. Single-scattering and optical properties of hexagonal ice crystals. *J. Atmos. Sci.*, **46,** 3–19.

Tao, W. K., J. Simpson, and S. T. Soong, 1991: Numerical simulation of a subtropical squall line over the Taiwan Strait. *Mon. Wea. Rev.*, **119,** 2699–2723.

——, ——, C. H. Sui, B. Ferrier, S. Lang, J. Scala, M.-D. Chou, and K. Pickering, 1993: Heating, moisture and water budgets of tropical and midlatitude squall lines: Comparisons and sensitivity to longwave radiation. *J. Atmos. Sci.*, **50,** 673–690.

Wong, T., and G. L. Stephens, 1994: A numerical study on the interactions between tropical cloud clusters, radiation, and dynamics. Preprints, *Sixth Conf. on Climate Variations.* Nashville, TN, Amer. Meteor. Soc., 307–312.

Xu, K. M., and S. K. Krueger, 1991: Evaluation of cloudiness parameterizations using a cumulus ensemble model. *Mon. Wea. Rev.*, **119,** 342–367.

——, and D. A. Randall, 1995: Impact of interactive radiative transfer on the macroscopic behavior of explicitly simulated cumulus ensembles. *J. Atmos. Sci.*, **52,** 785–799.

——, A. Arakawa, and S. K. Krueger, 1992: The macroscopic behavior of cumulus ensembles simulated by a cumulus ensemble model. *J. Atmos. Sci.*, **49,** 2402–2420.

Yanai, M., S. Esbensen, and J. Chu, 1973: Determination of average bulk properties of tropical cloud clusters from large-scale heat and moisture budgets. *J. Atmos. Sci.*, **30,** 611–627.

——, ——, and ——, 1976: Response of deep and shallow tropical maritime cumuli to large-scale processes. *J. Atmos. Sci.*, **33,** 976–991.

Zipser, E. J., 1977: Mesoscale and convective-scale downdrafts as distinct components of squall-line structure. *Mon. Wea. Rev.*, **105,** 1568–1589.